RESEARCH ARTICLE
doi: 10.2306/scienceasia1513-1874.2024.012

ScienceAsia 50 (3): 2024: ID 2024012: **1–9**

Dependence of initial value and adaptive adjustment on pattern formation for the coupled discrete diffusion system

Li Xu[a,b], **Jing Du**[c,*]

[a] School of Technology, Lishui University, Lishui 323000 China
[b] School of Science, Tianjin University of Commerce, Tianjin 300130 China
[c] School of Medicine, Lishui University, Lishui 323000 China

*Corresponding author, e-mail: bettyhappy409@163.com

Received 4 Aug 2022, Accepted 2 Sep 2023
Available online 23 Jan 2024

ABSTRACT: Turing patterns formation may depend on variation of the initial conditions. In this work, the dependent mechanism of initial distributions on pattern formation for the coupled discrete diffusion system is discussed, some asymptotic behavior between pattern formation and initial value determined by the corresponding eigenvectors of the eigenvalue for discrete Laplace operator can be given. To control the coupled discrete diffusion system for pattern selection, an adaptive adjustment mechanism is applied, and some theoretical generalizations are obtained. Then, the effectiveness of the theory analysis is validated though simulation results.

KEYWORDS: coupled discrete diffusion system, dependence of initial distributions, adaptive adjustment

MSC2020: 39A14 93D20

INTRODUCTION

Since the pioneering theoretical works of Turing [1], pattern dynamics, which can reflect the structural changes between various elements in the dynamic continuous or discrete reaction-diffusion systems, has become a very active research field. It is an essential branch of the nonlinear science and is applied in various aspects of physics, chemistry, biology and information science, see e.g. [2–10] and references therein. A nonlinear system is asymptotically stable when there is no diffusion, but becomes unstable when the diffusion is presented. This phenomenon is called diffusion-driven instability (Turing instability). Most numerical simulations of continuous or discrete reaction-diffusion models on pattern formation have used small random perturbations about the kinetic steady state as initial data, the steady state is stable to fluctuations but a parameter slowly changes, moving the system into the Turing space where Turing instability occurs. Some good numerical techniques are also applied to approximate the continuous Turing systems [11–13]. For example, a 2-D reaction diffusion equation is solved with the help of cubic B-spline quasi-interpolation method, and various patterns are captured in [13].

It is acceptable that Turing patterns formation may depend on not only fluctuation of system parameters but variation of the initial conditions. Indeed, both natural and social phenomena can be affected in some ways by the fluctuation of initial data. For some phenomena, such as harmonic oscillation, the dependence mechanism on initial conditions is very simple, but when damped, the dependence mechanism on initial values will become very complex, which has been verified by experiments and numerical simulations [11–18]. Murray [19] points out that, under zero flux conditions, for Turing-type reaction-diffusion equations, such as Thomas, Gierer-Meinhardt, Schnakenberg and other one-dimensional spatial variable models, both the solution patterns obtained and the patterns' polarity are sensitive to changes in the initial conditions and in the model domain's size and shape. In the study on the initial value dependence of local traveling wave convection pattern selection of mixed fluid in [20], the numerical results show that the dependence of traveling wave evolution on initial value is different under different conditions. Different initial distributions can result into different spatial distribution structures [8, 21–23], especially, when selecting some special initial values, there are obviously different spatial patterns [8, 21]. Although the following viewpoint is put forward in [24]: "It is observable that initial host patterns are different in each case but the long-time patterns are qualitatively the same", it should be noted that the spatial distribution of patterns may be significantly different although different initial conditions generate similar pattern structures, such as spiral patterns or chaotic patterns. Similar phenomena also appear in [25, 26].

The researches mentioned above have verified the relationship between the system evolution or pattern generation and the initial value (initial distribution) from the perspective of experiment or numerical simulation, which implies whether the pattern evolution continuously depends on the initial value or is sensitive to the initial value, whether the generated pattern has similarity or variability. Therefore, the study of

the mathematical mechanism of the pattern evolution affected by the initial value has attracted the attention of some scholars. For discrete systems, Xu et al [27] considered a two-dimensional logistic coupled map lattice with the periodic boundary conditions, in which any initial value can be linear expressed by corresponding eigenvectors for discrete Laplace operator, some asymptotic behavior between pattern formation and initial value determined by the corresponding eigenvectors of the eigenvalue can be found out. Similar methods were applied for a single-handed discrete Fisher equation in [28]. The above research deals with single equation discrete models. For the coupling discrete diffusion case, does the pattern evolution also have similar characteristics? Thus, in this paper, We will attempt to answer this question.

If the diffusion-driven instability should be avoided in some situations, and one may wish recovery stability towards the desired orbit, or one wish alter pattern evolution aim, such as from strip-like pattern to spot-like structure, some measures should be adopted to achieve the aim. Adaptive adjustment mechanism or the learning rules will be an effective one and need not alter the positions of positive equilibrium, which utilizes neither prior knowledge of the system itself nor extra external control signals, and forces all one-dimensional discrete systems to converge to their original periodic orbits [29]. The method is based on linearizing the system in a neighborhood of a fixed point and evaluating the eigenvalues of the corresponding Jacobian matrix, and is easy to implement. Then, it is often used for both discrete systems and continuous ones [30–33]. Motivated by adaptive adjustment mechanism, we will apply it to the coupled discrete diffusion system with the periodic boundary conditions to achieve the target of pattern selection, and hope to give some new generalizations for better interpretation and application on the adaptive adjustment mechanism.

So this paper is organized as follows. In the second section, we show how the different initial distributions have differential effects on the spatiotemporal dynamics of the coupled discrete diffusion system, some asymptotic behavior between pattern formation and initial value determined by the corresponding eigenvectors of the eigenvalue for discrete Laplace operator can be found. Furthermore, a discrete Lotka-Volterra cooperative system with the periodic boundary conditions model is used as an example to investigate the pattern selection with different initial value. Subsequently, in the third section, an adaptive adjustment mechanism is used to control the coupled discrete diffusion system for pattern selection, and obtain its stability conditions. Furthermore, some theoretical generalizations on the adaptive adjustment mechanism are shown, then we perform numerical simulations of the adjustment discrete Lotka-Volterra cooperative system for pattern formation. We summarize the main research contents and draw conclusions in the last section.

DEPENDENCE ON INITIAL VALUE

In this section, the following spatiotemporal discrete diffusion systems are considered:

$$\begin{cases} x_{ij}^{n+1} = f(x_{ij}^n, y_{ij}^n) + D_1 \nabla^2 x_{ij}^n, \\ y_{ij}^{n+1} = g(x_{ij}^n, y_{ij}^n) + D_2 \nabla^2 y_{ij}^n, \end{cases} \tag{1}$$

with periodic boundary conditions

$$\begin{cases} x_{i,0}^n = x_{i,m}^n, & x_{i,1}^n = x_{i,m+1}^n, \\ x_{0,j}^n = x_{m,j}^n, & x_{1,j}^n = x_{m+1,j}^n, \\ y_{i,0}^n = y_{i,m}^n, & y_{i,1}^n = y_{i,m+1}^n, \\ y_{0,j}^n = y_{m,j}^n, & y_{1,j}^n = y_{m+1,j}^n, \end{cases} \tag{2}$$

where $i, j \in \{1, 2, \cdots, m\} = [1, m]$, $n \in \mathbb{Z}^+$, m is a positive integer, D_1, $D_2 > 0$ are diffusion parameters, f and g are reaction functions, and ∇^2 is discrete Laplace operator defined as follows

$$\nabla^2 x_{ij}^n = x_{i+1,j}^n + x_{i,j+1}^n + x_{i-1,j}^n + x_{i,j-1}^n - 4x_{ij}^n, \tag{3}$$

$$\nabla^2 y_{ij}^n = y_{i+1,j}^n + y_{i,j+1}^n + y_{i-1,j}^n + y_{i,j-1}^n - 4y_{ij}^n. \tag{4}$$

Dependence analysis on initial value

Let the point $E^* = (x^*, y^*)$ is a positive equilibrium of (1), and still denote $x_{ij}^n - x^*$, $y_{ij}^n - y^*$ as x_{ij}^n, y_{ij}^n separately, then the linearization equation of (1) about E^* can be written as

$$\begin{cases} x_{ij}^{n+1} = f_{x^*} x_{ij}^n + f_{y^*} y_{ij}^n + D_1 \nabla^2 x_{ij}^n, \\ y_{ij}^{n+1} = g_{x^*} x_{ij}^n + g_{y^*} y_{ij}^n + D_2 \nabla^2 y_{ij}^n, \end{cases} \tag{5}$$

or

$$\begin{pmatrix} x_{ij}^{n+1} \\ y_{ij}^{n+1} \end{pmatrix} = \begin{pmatrix} f_{x^*} & f_{y^*} \\ g_{x^*} & g_{y^*} \end{pmatrix} \begin{pmatrix} x_{ij}^n \\ y_{ij}^n \end{pmatrix} + \begin{pmatrix} D_1 & 0 \\ 0 & D_2 \end{pmatrix} \begin{pmatrix} \nabla^2 x_{ij}^n \\ \nabla^2 y_n^{ij} \end{pmatrix},$$

where $f_{x^*} = \frac{\partial f}{\partial x}\,|_{(x^*,y^*)}$, $f_{y^*} = \frac{\partial f}{\partial y}\,|_{(x^*,y^*)}$, $g_{x^*} = \frac{\partial g}{\partial x}\,|_{(x^*,y^*)}$, $g_{y^*} = \frac{\partial g}{\partial y}\,|_{(x^*,y^*)}$.

In the view of [27], the eigenvalue problem

$$\begin{cases} \nabla^2 x_{ij} + \lambda x_{ij} = 0, \\ x_{0,j} = x_{m,j}, \quad x_{1,j} = x_{m+1,j}, \\ x_{i,0} = x_{i,m}, \quad x_{i,1} = x_{i,m+1}, \end{cases}$$

has the eigenvalues

$$\lambda_{kl} = 4\Big(\sin^2 \frac{(k-1)\pi}{m} + \sin^2 \frac{(l-1)\pi}{m}\Big), \quad k, l \in [1, m],$$

and the corresponding eigenfunctions

$$\varphi_{ij1}^{kl} = \sin\frac{2i(k-1)\pi}{m}\sin\frac{2j(l-1)\pi}{m},$$
$$\varphi_{ij2}^{kl} = \cos\frac{2i(k-1)\pi}{m}\cos\frac{2j(l-1)\pi}{m},$$
$$\varphi_{ij3}^{kl} = \sin\frac{2i(k-1)\pi}{m}\cos\frac{2j(l-1)\pi}{m},$$
$$\varphi_{ij4}^{kl} = \cos\frac{2i(k-1)\pi}{m}\sin\frac{2j(l-1)\pi}{m}.$$

Then, respectively taking the inner product of (5) with the corresponding eigenfunction φ_{ij}^{kl} of the eigenvalue λ_{kl}, we can obtain

$$\sum_{i,j=1}^{m}\varphi_{ij}^{kl}x_{ij}^{n+1} = f_{x^*}\sum_{i,j=1}^{m}\varphi_{ij}^{kl}x_{ij}^{n} + f_{y^*}\sum_{i,j=1}^{m}\varphi_{ij}^{kl}y_{ij}^{n} + D_1\sum_{i,j=1}^{m}\varphi_{ij}^{kl}\nabla^2 x_{ij}^{n},$$
$$\sum_{i,j=1}^{m}\varphi_{ij}^{kl}y_{ij}^{n+1} = g_{x^*}\sum_{i,j=1}^{m}\varphi_{ij}^{kl}x_{ij}^{n} + g_{y^*}\sum_{i,j=1}^{m}\varphi_{ij}^{kl}y_{ij}^{n} + D_2\sum_{i,j=1}^{m}\varphi_{ij}^{kl}\nabla^2 y_{ij}^{n}.$$

Let $U^n = \sum_{i,j=1}^{m}\varphi_{ij}^{kl}x_{ij}^{n}$, $V^n = \sum_{i,j=1}^{m}\varphi_{ij}^{kl}y_{ij}^{n}$, we can get

$$U^{n+1} = f_{x^*}U^n + f_{y^*}V^n - D_1\lambda_{kl}U^n,$$
$$V^{n+1} = g_{x^*}U^n + g_{y^*}V^n - D_2\lambda_{kl}V^n,$$

or

$$\begin{pmatrix}U^{n+1}\\V^{n+1}\end{pmatrix} = \begin{pmatrix}1-x^*-D_1\lambda_{kl} & a_{12}x^*\\ a_{21}y^* & 1-y^*-D_2\lambda_{kl}\end{pmatrix}\begin{pmatrix}U^n\\V^n\end{pmatrix}.$$

Let

$$A = \begin{pmatrix}f_{x^*}-D_1\lambda_{kl} & f_{y^*}\\ g_{x^*} & g_{y^*}-D_2\lambda_{kl}\end{pmatrix},$$

its eigenvalues are

$$\lambda_+(k,l) = \frac{1}{2}\mathrm{tr}(k,l) + \frac{1}{2}\sqrt{\mathrm{tr}(k,l)^2 - 4\triangle(k,l)},$$
$$\lambda_-(k,l) = \frac{1}{2}\mathrm{tr}(k,l) - \frac{1}{2}\sqrt{\mathrm{tr}(k,l)^2 - 4\triangle(k,l)},$$

where

$$\mathrm{tr}(k,l) = f_{x^*} + g_{y^*} - (D_1+D_2)\lambda_{kl},$$
$$\triangle(k,l) = f_{x^*}g_{y^*} - f_{y^*g_{x^*}} - (D_1g_{y^*} + D_2f_{x^*})\lambda_{kl} + D_1D_2\lambda_{kl}^2.$$

Let

$$x_{ij}^0 = \sum_{k,l=1}^{m}c_{kl}\varphi_{ij}^{kl}, \quad y_{ij}^0 = \sum_{k,l=1}^{m}d_{kl}\varphi_{ij}^{kl},$$

there exists an invertible matrix P such that

$$A = P^{-1}\begin{pmatrix}\lambda_+(k,l) & 0\\ 0 & \lambda_-(k,l)\end{pmatrix}P$$

holds. Then

$$\begin{pmatrix}x_{ij}^n\\y_{ij}^n\end{pmatrix} = A^n\begin{pmatrix}x_{ij}^0\\y_{ij}^0\end{pmatrix} = P^{-1}\begin{pmatrix}\lambda_+^n(k,l) & 0\\ 0 & \lambda_-^n(k,l)\end{pmatrix}P\begin{pmatrix}x_{ij}^0\\y_{ij}^0\end{pmatrix}.$$

Let

$$\lambda_M(k,l) = \max_{k=1,l=1}^{m}\{|\lambda_+(k,l)|, |\lambda_-(k,l)|\},$$
$$\lambda_{KL} = \max_{k=1,l=1}^{m}\lambda_M(k,l),$$

we can obtain

$$\frac{1}{\lambda_{KL}^n}\begin{pmatrix}x_{ij}^n\\y_{ij}^n\end{pmatrix} = P^{-1}\begin{pmatrix}\frac{\lambda_+^n(k,l)}{\lambda_{KL}^n} & 0\\ 0 & \frac{\lambda_-^n(k,l)}{\lambda_{KL}^n}\end{pmatrix}P\begin{pmatrix}x_{ij}^0\\y_{ij}^0\end{pmatrix} = P^{-1}\begin{pmatrix}\frac{\lambda_+^n(k,l)}{\lambda_{KL}^n} & 0\\ 0 & \frac{\lambda_-^n(k,l)}{\lambda_{KL}^n}\end{pmatrix}P\begin{pmatrix}\sum_{k,l=1}^{m}c_{kl}\varphi_{ij}^{kl}\\ \sum_{k,l=1}^{m}d_{kl}\varphi_{ij}^{kl}\end{pmatrix} \sim \begin{pmatrix}c_{KL}\varphi_{ij}^{KL}\\ d_{KL}\varphi_{ij}^{KL}\end{pmatrix}. \tag{6}$$

Remark 1 From above discussion, we find that the solution $\begin{pmatrix}x_{ij}^n\\y_{ij}^n\end{pmatrix}_{i,j\in[1,m]}^{n\in Z^+}$ of the system (1)–(4) and the sequence $\lambda_{KL}^n\begin{pmatrix}c_{KL}\varphi_{ij}^{KL}\\ d_{KL}\varphi_{ij}^{KL}\end{pmatrix}_{i,j\in[1,m]}^{n\in Z^+}$ have some asymptotic behavior.

Example

In the subsection, we will perform a series of numerical simulations to verify the above theoretical analysis. For simplicity, we consider the following discrete Lotka-Volterra cooperative system with the periodic boundary conditions

$$\begin{cases}x_{ij}^{n+1} = x_{ij}^n\exp(r - x_{ij}^n + ay_{ij}^n) + D\nabla^2 x_{ij}^n,\\ y_{ij}^{n+1} = y_{ij}^n\exp(r + ax_{ij}^n - y_{ij}^n) + D\nabla^2 y_{ij}^n.\end{cases} \tag{7}$$

Turing instability conditions on the system (7) have been presented by Xu et al [34], namely, if $0 < r < 2$, $0 < a < 1$ and there exists the positive constant D such that

$$\lambda_{kl} > \frac{1}{D}\Big(2 - \frac{r(1+a)}{1-a}\Big),$$

holds, then the symmetric discrete system (7) is Turing unstable at the positive fixed point $E = (\frac{r}{1-a}, \frac{r}{1-a})$. It also means that

$$\lambda_{k+\tau,l+\iota} > \tfrac{1}{D}\big(2 - \tfrac{r(1+a)}{1-a}\big),\ (\tau,\iota)\in[0,m-2k]\times[0,m-2l].$$

Thus, the initial values v_{ij}^0, y_{ij}^0 should be chosen by

$$x_{ij}^0 = \frac{r}{1-a} + \varepsilon_1 \sum_{\tau=0}^{m-2k} \sum_{\iota=0}^{m-2l} c_{\tau\iota} \varphi_{ij}^{k+\tau,l+\iota},$$
$$y_{ij}^0 = \frac{r}{1-a} + \varepsilon_2 \sum_{\tau=0}^{m-2k} \sum_{\iota=0}^{m-2l} d_{\tau\iota} \varphi_{ij}^{k+\tau,l+\iota},$$

where ε_1 and ε_2 are sufficiently small. Let

$$D > \frac{1}{\lambda_{kl}}\Big(2 - \frac{r(1+a)}{1-a}\Big) = \frac{1}{4\sin^2\frac{\pi}{201}}\Big(2 - \frac{r(1+a)}{1-a}\Big),$$

then, for any $(k,l) \in [1,m]\times[2,m]$ or $(k,l) \in [2,m]\times[1,m]$, λ_{kl} satisfies the Turing instability condition. If we choose $r = 1.1, a = 0.2$, then

$$D > \frac{1}{4\sin^2\frac{\pi}{201}}\Big(2 - \frac{r(1+a)}{1-a}\Big) \approx 358.21.$$

In this case, we choose that $D = 400$, $m = 201$ and

$$x_{ij}^0 = \tfrac{r}{1-a} + 0.01\sin\tfrac{2i\pi}{201}\sin\tfrac{2j\pi}{201} + 0.01\sin\tfrac{4i\pi}{201}\sin\tfrac{4j\pi}{201}, \quad (8)$$
$$y_{ij}^0 = \tfrac{r}{1-a} + 0.01\sin\tfrac{2i\pi}{201}\sin\tfrac{2j\pi}{201} + 0.01\sin\tfrac{4i\pi}{201}\sin\tfrac{4j\pi}{201}, \quad (9)$$

for simulations, a spatial-like pattern is shown in Fig. 1(a), which is highly similar with the pattern (Fig. 1(b)) generated when the initial value is selected as follows.

$$x_{ij}^0 = \frac{r}{1-a} + 0.01\sin\frac{4i\pi}{201}\sin\frac{4j\pi}{201}, \quad (10)$$
$$y_{ij}^0 = \frac{r}{1-a} + 0.01\sin\frac{4i\pi}{201}\sin\frac{4j\pi}{201}. \quad (11)$$

Suppose that

$$\lambda_{KL} > \frac{1}{D}\Big(2 - \frac{r(1+a)}{1-a}\Big),$$

and

$$\lambda_{kl} < \frac{1}{D}\Big(2 - \frac{r(1+a)}{1-a}\Big), (k,l) \neq (K,L),$$

in which $(K,L) = (\frac{m+1}{2}, \frac{m+1}{2})$, if m is odd; $(K,L) = (\frac{m}{2}+1, \frac{m}{2}+1)$, if m is even. In this case, we can choose the initial values distribution

$$x_{ij}^0 = \frac{r}{1-a} + \varepsilon_1\varphi_{ij}^{KL}, \quad y_{ij}^0 = \frac{r}{1-a} + \varepsilon_2\varphi_{ij}^{KL}.$$

Let $m = 201$, then

$$\lambda_{kl} = 4\Big(\sin^2\frac{(k-1)\pi}{201} + \sin^2\frac{(l-1)\pi}{201}\Big), \quad k,l \in [1,m],$$

$$\lambda_{101,101} = 4\Big(\sin^2\tfrac{(100)\pi}{201} + \sin^2\frac{(100)\pi}{201}\Big) = 7.9995,$$

and

$$\lambda_{101,100} = \lambda_{100,101} = 4\Big(\sin^2\tfrac{(100)\pi}{201} + \sin^2\tfrac{(99)\pi}{201}\Big) = 7.9976.$$

Let $r = 1.1$, $a = 0.2$, and suppose that

$$7.9976 < \frac{1}{D}\Big(2 - \frac{r(1+a)}{1-a}\Big) < 7.9995,$$

then

$$0.20626 < D < 0.20631.$$

We choose $D = 0.20628$ and

$$x_{ij}^0 = \frac{r}{1-a} + 0.001\sin\tfrac{2i(101-1)\pi}{201}\sin\tfrac{2j(101-1)\pi}{201}, \quad (12)$$
$$y_{ij}^0 = \frac{r}{1-a} + 0.001\sin\tfrac{2i(101-1)\pi}{201}\sin\tfrac{2j(101-1)\pi}{201}, \quad (13)$$

spiral pattern will emerge in Fig. 2(a). Furthermore, we choose $D = 0.20629$ and $D = 0.20630$, the corresponding spatial structures (Fig. 2(b) and Fig. 2(c)) are also similar with Fig. 2(a). Therefore, it can be judged numerically that if the parameters r and a are kept fixed in the Turing instability region, and the initial values are also fixed, the patterns generated in the interval $0.20626 < D < 0.20631$ have similarity.

Through the previous discussion of eigenvalue problem, we found that the same eigenvalue will correspond to different eigenfunctions. In order to numerically verify the pattern formation results caused by different eigenfunctions, the following initial values are selected.

$$x_{ij}^0 = \frac{r}{1-a} + 0.001\cos\tfrac{2i(101-1)\pi}{201}\cos\tfrac{2j(101-1)\pi}{201}, \quad (14)$$
$$y_{ij}^0 = \frac{r}{1-a} + 0.001\cos\tfrac{2i(101-1)\pi}{201}\cos\tfrac{2j(101-1)\pi}{201}. \quad (15)$$

with $r = 1.1, a = 0.2, D = 0.20628$. From Fig. 3, we can find out that, if the initial values distribution are chosen as (14)–(15) and (12)–(13), respectively, although the spiral structure will also be generated, there will be great differences in spatial distribution, especially in the evolution process. Therefore, it can be judged numerically that, if the system parameters are fixed and different eigenvectors corresponding to the same eigenvalue are selected as the initial values, the resulting patterns may have certain differences.

Next, we fix the parameters $r = 1.1$, $a = 0.2$, $D = 0.20628$, and change the number of spatial grids, take $m = 200$ and $m = 201$ separately. It can be observed that the generated patterns are significantly different, see Fig. 4. It is because, if $m = 200$, then

$$\lambda_{kl} = 4\Big(\sin^2\tfrac{(k-1)\pi}{200} + \sin^2\tfrac{(l-1)\pi}{200}\Big), \quad k,l \in [1,m],$$

$$\lambda_{101,101} = 4\Big(\sin^2\tfrac{(101-1)\pi}{200} + \sin^2\tfrac{(101-1)\pi}{200}\Big) = 8,$$
$$\lambda_{101,100} = 4\Big(\sin^2\tfrac{(101-1)\pi}{200} + \sin^2\tfrac{(100-1)\pi}{200}\Big) = 7.999.$$

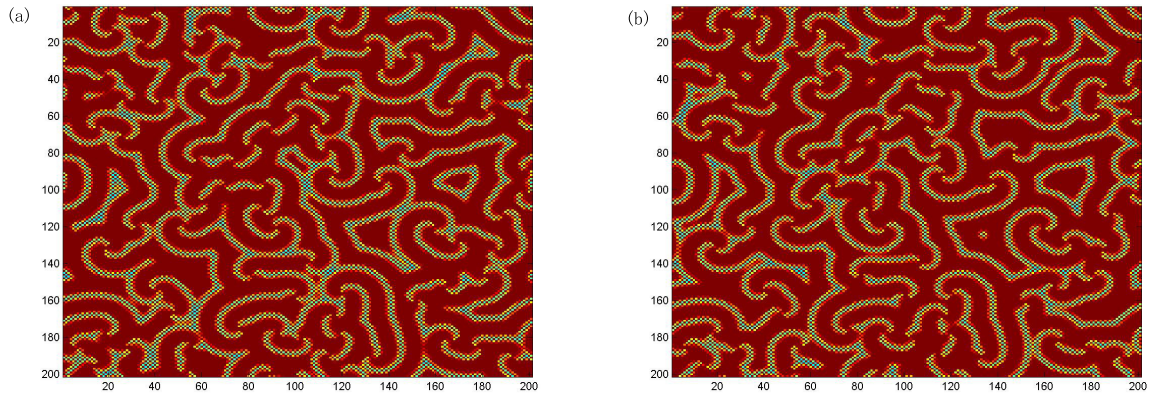

Fig. 1 Selective patterns for x, when $r = 1.1$, $a = 0.2$, $D = 360$. (a) $n = 50000$, the initial values distribution is chosen as (8). (b) $n = 50000$, the initial values distribution is chosen as (10).

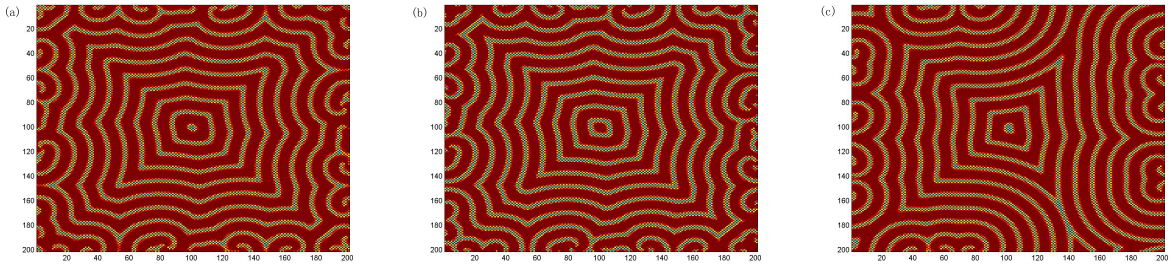

Fig. 2 Snapshots of contour pictures of the time evolution on x, when $r = 1.1$, $a = 0.2$. (a) $D = 0.20628$, $n = 50000$. (b) $D = 0.20629$, $n = 50000$. (c) $D = 0.20630$, $n = 50000$.

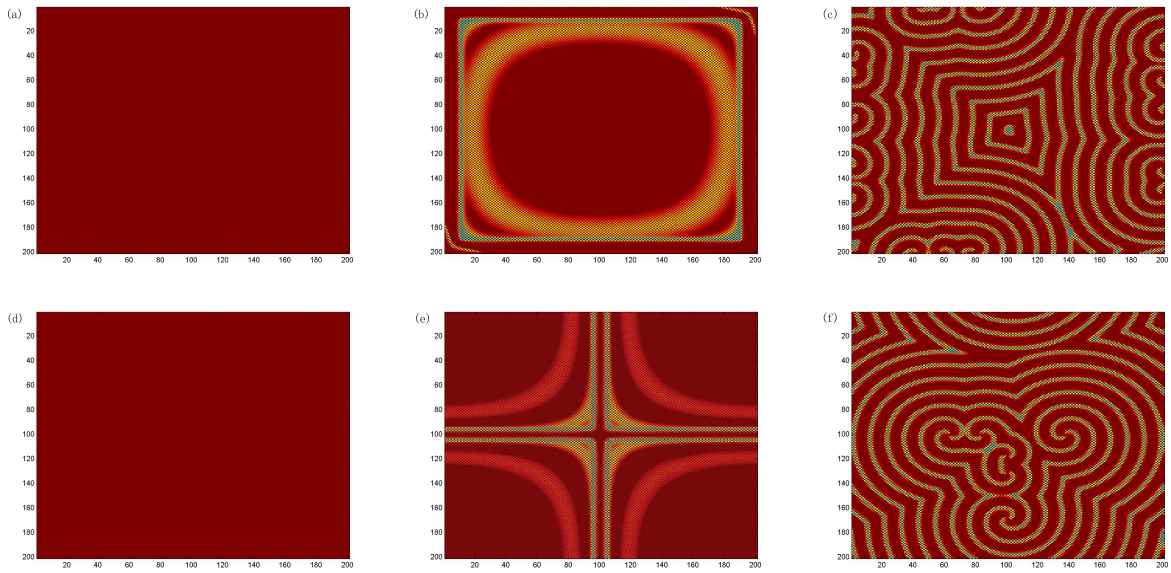

Fig. 3 Selective patterns on x resulting from different eigenfunctions, when $r = 1.1$, $a = 0.2$, $D = 0.20628$. (a) $n = 1$, the initial values distribution is chosen as (12). (b) $n = 100$, the initial values distribution is chosen as (12). (c) $n = 50000$, the initial values distribution is chosen as (12). (d) $n = 1$, the initial values distribution is chosen as (14). (e) $n = 100$, the initial values distribution is chosen as (14). (f) $n = 50000$, the initial values distribution is chosen as (14).

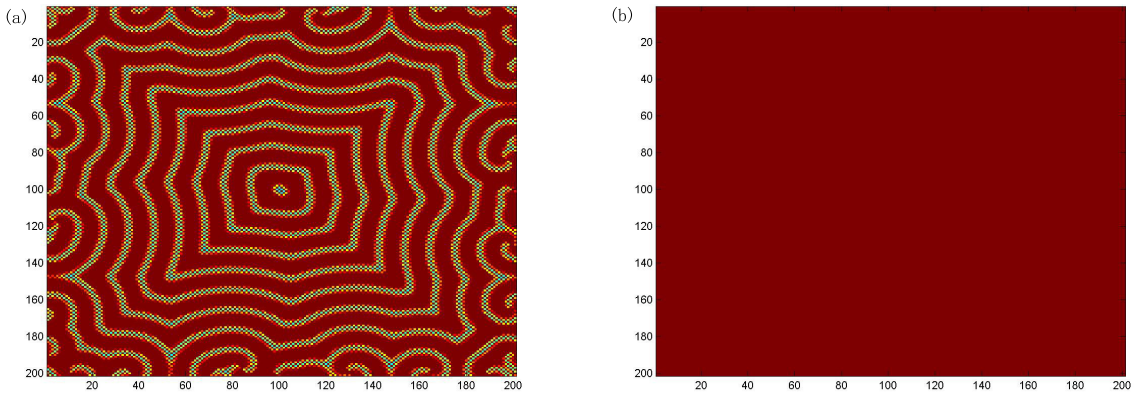

Fig. 4 Selective patterns on x for different m, when $r = 1.1$, $a = 0.2$, $D = 0.20628$. (a) $n = 50000$, $m = 201$. (b) $n = 50000$, $m = 200$.

If still take $r = 1.1$, $a = 0.2$, and

$$7.999 < \frac{1}{D}\Big(2 - \frac{r(1+a)}{1-a}\Big) < 8,$$

then

$$0.20625 < D < 0.2062576.$$

We find out that the parameter $D = 0.20628$ does not meet the Turing instability condition when $m = 200$, but falls in the stable region, so the symmetry breaking does not occur. At this time, we can infer that when m is selected differently, the eigenvalue and eigenvector have changed, and the corresponding iteration matrix has also changed. Therefore, although the same parameters are selected, the differential patterns may occur.

ADAPTIVE ADJUSTMENT ON PATTERN FORMATION

Adaptive adjustment method is a control strategy in which state feedback method and parameter perturbation are combined and used to stabilize instability or chaos system [29–32]. So that, for a large range of parameter the controlled system maintain its stability. Now, deploying adaptive adjustment mechanism to the system (1)–(2), we can obtain the corresponding controlled system,

$$\begin{cases} x_{ij}^{n+1} = \gamma_1(f(x_{ij}^n, y_{ij}^n) + D_1\nabla^2 x_{ij}^n) + (1-\gamma_1)x_{ij}^n, \\ y_{ij}^{n+1} = \gamma_2(g(x_{ij}^n, y_{ij}^n) + D_2\nabla^2 y_{ij}^n) + (1-\gamma_2)y_{ij}^n, \end{cases} \tag{16}$$

with periodic boundary conditions

$$\begin{cases} x_{i,0}^n = x_{i,m}^n,\ x_{i,1}^n = x_{i,m+1}^n, \\ x_{0,j}^n = x_{m,j}^n,\ x_{1,j}^n = x_{m+1,j}^n, \\ y_{i,0}^n = y_{i,m}^n,\ y_{i,1}^n = y_{i,m+1}^n, \\ y_{0,j}^n = y_{m,j}^n,\ y_{1,j}^n = y_{m+1,j}^n, \end{cases} \tag{17}$$

where γ_1, γ_2 are the adjustment parameters. If $\gamma_1 \neq \gamma_2$, the mechanism is called nonuniformly adaptive adjustment, if $\gamma_1 = \gamma_2$, it is called uniformly adaptive adjustment. At $\gamma_1, \gamma_2 = 0$, the controlled system (16) becomes the original system (7).

Stability analysis

The discrete systems can be stabilized by an adaptive adjustment [29, 30], then the stability analysis on system (16)–(17) can also be done. For simplicity, the detailed calculation is given through an example in the next subsection. However, we find out the following fact in this subsection.

Fix $k, l \in \mathbb{N}$ and assume that T is nonexpansive mapping on a closed convex subset $D \subset \mathbb{R}^n$. Defined a sequence $\{x_t\}$ in D by $x_1, x_2, \ldots, x_{\max\{k,l\}} \in D$ and

$$x_t = \lambda T x_{t-k} + (1-\lambda)x_{t-l} \tag{18}$$

for $t \in \mathbb{N}$ with $t > \max\{k, l\}$. Under a suitable assumption, does $\{x_t\}$ converge to a fixed point of T? We can get the following conclusion.

Proposition 1 *Fix $k, l \in \mathbb{N}$, put $m = \max k, l$. Let D be the unit ball of the 2-dimensional real Hilbert space E. If $l \neq 1$, then for any $\lambda > 0$ there exists a nonexpansive mapping T on D and a sequence $\{x_t\}$ such that $\{x_t\}$ dose not converge.*

Proof: Put $m = \max\{k, l\}$. Define a nonexpansive mapping T by

$$T(u_1, u_2) = \Big(u_1 \cos\tfrac{2\pi k}{l} - u_2 \sin\tfrac{2\pi k}{l}, u_1 \sin\tfrac{2\pi k}{l} + u_2 \cos\tfrac{2\pi k}{l}\Big)$$

for $(u_1, u_2) \in D$. Set $x_1, x_2, \cdots, x_m \in D$ by

$$x_j = (\cos\tfrac{2\pi j}{l}, \sin\tfrac{2\pi j}{l}), \quad j = 1, 2, \ldots, m.$$

We shall show

$$x_j = (\cos\tfrac{2\pi j}{l}, \sin\tfrac{2\pi j}{l}) \quad \text{for all } j \in \mathbb{N}.$$

It holds when $j \leqslant m$. We assume that $t > m$ and the equation holds for $j < t$. Then we have

$$\begin{aligned} x_t &= \lambda T x_{t-k} + (1-\lambda) x_{t-k} \\ &= \lambda T \left(\cos \tfrac{2\pi(t-k)}{l}, \sin \tfrac{2\pi(t-k)}{l}\right) \\ &\quad + (1-\lambda)\left(\cos \tfrac{2\pi(t-k)}{l}, \sin \tfrac{2\pi(t-l)}{l}\right) \\ &= \lambda \left(\cos \tfrac{2\pi(t-k+k)}{l}, \sin \tfrac{2\pi(t-k+k)}{l}\right) \\ &\quad + (1-\lambda)\left(\cos \tfrac{2\pi t}{l}, \sin \tfrac{2\pi t}{l}\right) \\ &= \left(\cos \tfrac{2\pi t}{l}, \sin \tfrac{2\pi t}{l}\right). \end{aligned}$$

By induction,we obtain the equation. This completes the proof. □

Remark 2 Proposition 1 implies that the adaptive adjustment or learning rule system of the form

$$x_{t+1} = \lambda T x_t + (1-\lambda) x_{t-l}$$

can be unstable when $l \geqslant 1$.

Simulations

As an example, we consider the following discrete control system with the periodic boundary conditions.

$$\begin{cases} x_{ij}^{n+1} = \gamma(x_{ij}^n \exp(r - x_{ij}^n + a y_{ij}^n) + D\nabla^2 x_{ij}^n) + (1-\gamma) x_{ij}^n, \\ y_{ij}^{n+1} = \gamma(y_{ij}^n \exp(r + a x_{ij}^n - y_{ij}^n) + D\nabla^2 y_{ij}^n) + (1-\gamma) y_{ij}^n. \end{cases} \tag{19}$$

Then we can deduce the symmetric discrete system with uniformly adaptive adjustment is stable at the positive fixed point $E = (\frac{r}{1-a}, \frac{r}{1-a})$ if and only if $0 < r < 2$, $0 < a < 1$ and there exists the nonnegative constant γ such that

$$0 < \gamma\Big(\frac{r(1+a)}{1-a} + D\lambda_{kl}\Big) < 2$$

holds. For its details, see the appendix.

We still assume that $r = 1.1$, $a = 0.2$, $D = 0.20628$, $m = 201$, and

$$\begin{aligned} x_{ij}^0 &= \frac{r}{1-a} + 0.001 \sin \tfrac{2i(101-1)\pi}{201} \sin \tfrac{2j(101-1)\pi}{201}, \\ y_{ij}^0 &= \frac{r}{1-a} + 0.001 \sin \tfrac{2i(101-1)\pi}{201} \sin \tfrac{2j(101-1)\pi}{201}, \end{aligned}$$

in this case, $\lambda_{101,101} = 4\Big(\sin^2 \frac{(101-1)\pi}{201} + \sin^2 \frac{(101-1)\pi}{201}\Big) = 7.9995$, then (19) is stable when $0.39396 < \gamma < 1$. We can observe that, with the iteration's further increased if $\gamma = 0.5$, the boundary of the domain moves in time till a single domain covers the space, whose pattern is similar with Fig. 4(b). Even if other parameter $\gamma \in (0.39396, 1)$ is selected, similar fact will be observed, which only has different single color to the whole domain. Next, we take $\gamma = 0.05$, which falls on the unstable region, the evolution pattern is shown in Fig. 5(a). The spiral-like pattern is observed, which is similar with Fig. 2(a). With the further increase of $\gamma \in (0, 0.39396)$, spiral patterns can still emerge, the density of the spirals will decrease, and there is a trend towards steady state, see Fig. 5(b) and Fig. 5(c). However, if $\gamma = 1.1$ which still falls on the unstable region, one can see that a single blue covers the whole space, which we call 'not good' pattern or 'overflowing' pattern (Fig. 5(d)).

To examine Proposition 1, we construct the following discrete control system with the periodic boundary conditions for simulations. Set $r = 1.1$, $a = 0.2$, $D = 0.20628$, $m = 201$, and

$$\begin{cases} x_{ij}^{n+1} = \gamma(x_{ij}^n \exp(r - x_{ij}^n + a y_{ij}^n) + D\nabla^2 x_{ij}^n) + (1-\gamma) x_{ij}^{n-1}, \\ y_{ij}^{n+1} = \gamma(y_{ij}^n \exp(r + a x_{ij}^n - y_{ij}^n) + D\nabla^2 y_{ij}^n) + (1-\gamma) y_{ij}^{n-1}. \end{cases}$$

We can find spiral-like patterns and 'overflowing' patterns can emerge, but steady state patterns can not be observed for all $\gamma > 0$.

CONCLUSION

We give several concluding remarks in this section.

1) Taking the coupled discrete diffusion equation as the research object, the relationship between the pattern evolution and the initial value is discussed. The analysis method is derived from [27], it is more general and suitable for high-dimensional situations. Indeed, in this work, theoretical analysis shows that taking the initial value in the Turing unstable selection region, the pattern generation is affected by the eigenfunction corresponding to the eigenvalue of the discrete Laplace operator with the largest modulus. Using the eigenfunction corresponding to this eigenvalue to select the initial value, we can obtain a pattern with certain characteristics. Numerical simulations verify the following conclusions:

(a) With fixed initial values, the parameter space can be obtained in the Turing unstable region, and the patterns generated in this parameter space have similarity.

(b) With fixed parameters, taking different eigenfunction corresponding to the same eigenvalue as the initial value, can lead to the difference of the generated pattern.

(c) With fixed parameters, when the spatial lattice division changes, the eigenvalues and eigenfunctions will change, and lead to the difference of the generated patterns.

2) We use adaptive adjustment mechanism to control the discrete Turing system, showing that the controlled system can select the pattern formation. In addition, some theoretical generalization on adaptive adjustment mechanism is obtained. The simulation result has also validated the effectiveness of the adaptive adjustment mechanism.

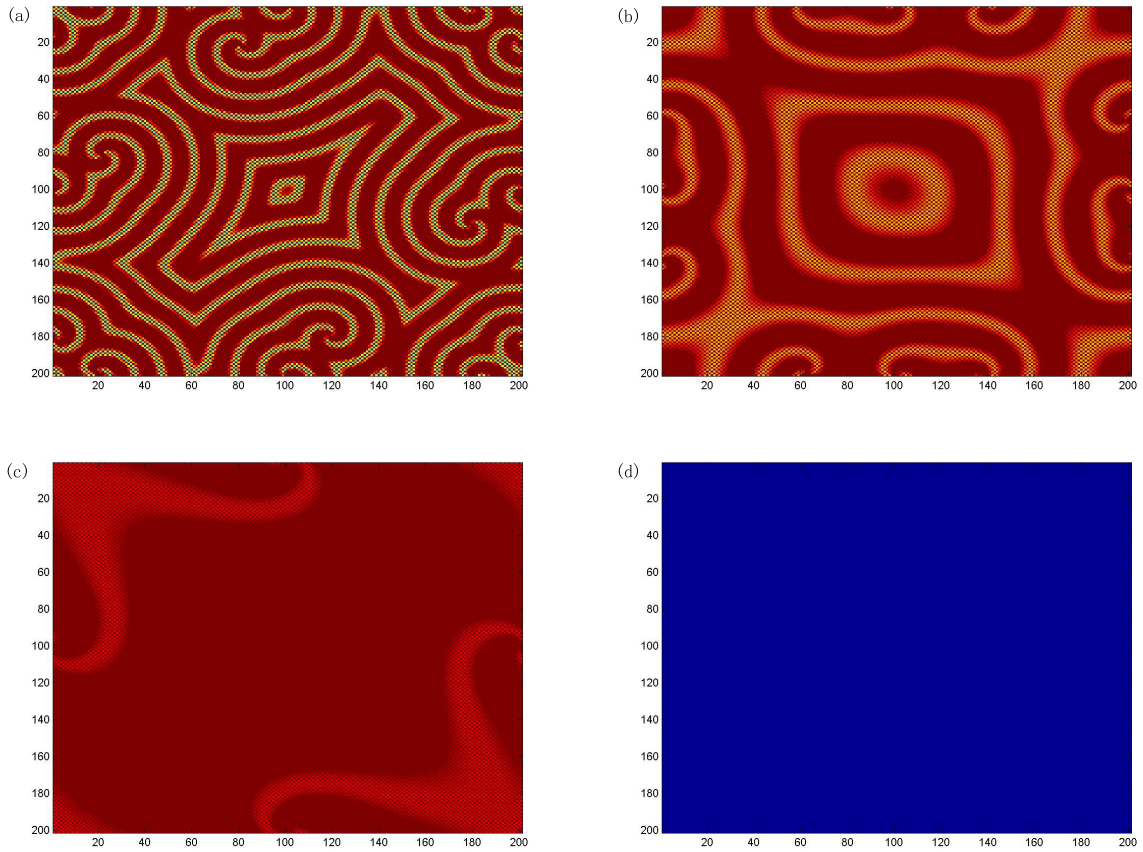

Fig. 5 Selective patterns on x for different γ, when $r = 1.1$, $a = 0.2$, $D = 0.20628$, $m = 201$, $n = 50000$. (a) $\gamma = 0.05$. (b) $\gamma = 0.15$. (c) $\gamma = 0.4$. (d) $\gamma = 1.1$.

Appendix

In this appendix, we discuss the instability of (19) with the periodic boundary conditions at the positive fixed point $E = (\frac{r}{1-a}, \frac{r}{1-a})$.

Then, the linearized form of (19) at $E = (\frac{r}{1-a}, \frac{r}{1-a})$ is

$$\begin{cases} x_{ij}^{n+1} = (1-\frac{r(1-\gamma)}{1-a})x_{ij}^n + \frac{r(1-\gamma)}{1-a}y_{ij}^n + D(1-\gamma)\nabla^2 x_{ij}^n, \\ y_{ij}^{n+1} = \frac{r(1-\gamma)}{1-a}x_{ij}^n + (1-\frac{r(1-\gamma)}{1-a})y_{ij}^n + D(1-\gamma)\nabla^2 y_{ij}^n. \end{cases} \tag{20}$$

Taking the inner product of (20) with the corresponding eigenfunction of the eigenvalue λ_{kl}, we see that

$$\begin{cases} \sum\limits_{i,j=1}^{m} \varphi_{ij}^{kl} x_{ij}^{n+1} = (1-\frac{r(1-\gamma)}{1-a}) \sum\limits_{i,j=1}^{m} \varphi_{ij}^{kl} x_{ij}^n + \frac{r(1-\gamma)}{1-a} \sum\limits_{i,j=1}^{m} \varphi_{ij}^{kl} y_{ij}^n \\ \qquad +D(1-\gamma) \sum\limits_{i,j=1}^{m} \varphi_{ij}^{kl} \nabla^2 x_{ij}^n, \\ \sum\limits_{i,j=1}^{m} \varphi_{ij}^{kl} y_{ij}^{n+1} = \frac{r(1-\gamma)}{1-a} \sum\limits_{i,j=1}^{m} \varphi_{ij}^{kl} x_{ij}^n + (1-\frac{r(1-\gamma)}{1-a}) \sum\limits_{i,j=1}^{m} \varphi_{ij}^{kl} y_{ij}^n \\ \qquad +D(1-\gamma) \sum\limits_{i,j=1}^{m} \varphi_{ij}^{kl} \nabla^2 y_{ij}^n. \end{cases} \tag{21}$$

Let $U^n = \sum\limits_{i,j=1}^{m} \varphi_{ij}^{kl} x_{ij}^n, V^n = \sum\limits_{i,j=1}^{m} \varphi_{ij}^{kl} y_{ij}^n$, and use the periodic boundary conditions (2), then we have

$$\begin{cases} U^{n+1} = (1-\frac{r(1-\gamma)}{1-a})U^n + \frac{r(1-\gamma)}{1-a}V^n - D(1-\gamma)\lambda_{kl}U^n, \\ V^{n+1} = \frac{r(1-\gamma)}{1-a}U^n + (1-\frac{r(1-\gamma)}{1-a})V^n - D(1-\gamma)\lambda_{kl}V^n. \end{cases} \tag{22}$$

If (U^n, V^n) is a solution of the system (22), then $(x_{ij}^n = U^n\varphi_{ij}^{kl},\ y_{ij}^n = V^n\varphi_{ij}^{kl})$ is also obviously a solution of (20) with the periodic boundary conditions. Thus, the stable system (22) will produce that the problem (20) is stable.

Let

$$J = \begin{pmatrix} (1-\frac{r(1-\gamma)}{1-a}) - D(1-\gamma)\lambda_{kl} & \frac{r(1-\gamma)}{1-a} \\ \frac{r(1-\gamma)}{1-a} & (1-\frac{r(1-\gamma)}{1-a}) - D(1-\gamma)\lambda_{kl} \end{pmatrix},$$

its eigenvalues are

$$\lambda_1(k,l) = 1-(1-m)D\lambda_{kl},$$
$$\lambda_2(k,l) = (1-m)\Big(1-\frac{r(1+a)}{1-a}-D\lambda_{kl}\Big)+m.$$

By means of $\left|\lambda_{1,2}(k,l)\right| < 1$, the stability conditions of the system (20) with periodic boundary conditions can be obtained.

Acknowledgements: The authors wish to express their gratitude to Professor Genqi Xu for his helpful comments and valuable suggestions with careful readings which greatly improved the quality of the paper.

REFERENCES

1. Turing AM (1952) The chemical basis of morphogenesis. *Philos T R Soc B* **237**, 37–72.
2. Crampin E, Hackborn W, Maini P (2002) Pattern formation in reaction-diffusion models with nonuniform domain growth. *B Math Biol* **64**, 747–769.
3. Kondo S, Miura T (2010) Reaction-diffusion model as a framework for understanding biological pattern formation. *Science* **329**, 1616–1620.
4. Economou AD, Ohazama A, Porntaveetus T, Sharpe PT, Kondo S, Basson MA, Gritli Linde A, Cobourne MT, Green JB (2012) Periodic stripe formation by a Turing mechanism operating at growth zones in the mammalian palate. *Nay Genet* **44**, 348–351.
5. Merle M, Messio L, Mozziconacci J (2022) Turing-like patterns in an asymmetric dynamic ising model. *Phys Rev E* **100**, 042111.
6. Anirban A (2022) 70 years of Turing patterns. *Nat Rev Phys* **4**, 432.
7. Hu JL, Zhu LH, Peng M (2022) Analysis of Turing patterns and amplitude equations in general forms under a reaction-diffusion rumor propagation system with Allee effect and time delay. *Inf Sci* **596**, 501–519.
8. Xu L, Zhang G, Han B, Zhang L, Li MF, Han YT (2010) Turing instability for a two-dimensional Logistic coupled map lattice. *Phys Lett A* **374**, 3447–3450.
9. Muzika F, Schreiberov L, Schreiber L (2020) Advanced chemical computing using discrete Turing patterns in arrays of coupled cells. *Front Chem* **8**, 559650.
10. Leyshon T, Tonello E, Schnoerr D, Siebert H, Stumpf MPH (2021) The design principles of discrete Turing patterning systems. *J Theor Biol* **531**, 110901.
11. Jiwari R, Singh S, Kumar A (2017) Numerical simulation to capture the pattern formation of coupled reaction-diffusion models. *Chaos Soliton Fract* **103**, 42—439.
12. Yadav OP, Jiwari R (2019) A finite element approach to capture Turing patterns of autocatalytic Brusselator model. *J Math Chem* **57**,769–789.
13. Mittal RC, Kumar S, Jiwari R (2022) A cubic B-spline quasi-interpolation algorithm to capture the pattern formation of coupled reaction diffusion models. *Eng Comput* **38**, 1375–1391.
14. Skudarnov PV, Lin CX, Wang MH, Pradeep N, Ebadian MA (2002) Evolution of convection pattern during the solidification process of a binary mixture: effect of initial solutal concentration. *Int J Heat Mass Tran* **45**, 5191–5200.
15. Luo AR, Li YC, Feng ZC, Fox NI, Rabinowitz JL, Simpson MJ, Talbot RW (2016) Sensitive versus rough dependence under initial conditions in atmospheric flow regimes. *Atmosphere-Basel* **7**, 157.
16. Alejandro CO, Sergio GS, Jose AF (2020) Non-linear evolutions of magnetized thick discs around black holes: dependence on the initial data. *Mon Not R Astron Soc* **492**,5730–5742.
17. Pandit S (2022) Local radial basis functions and scale-3 Haar wavelets operational matrices based numerical algorithms for generalized regularized long wave model. *Wave Motion* **109**, 102846.
18. Jiwari R, Kumar S, Mitta RC (2019) Meshfree algorithms based on radial basis functions for numerical simulation and to capture shocks behavior of Burgers' type problems. *Eng Computation* **36**,1142–1168.
19. Arcuri A, Murray D (1986) Pattern sensitivity to boundary and initial conditions in reaction-diffusion models. *J Math Biol* **24**, 141–165.
20. Ning LZ, Wu H, Ning BB, Yuan Z, Tian WL, Ning JH (2017) Initial-value dependence of pattern selection of localized traveling wave convection in a binary fluid mixture. *Chinese J Appl Mech* **34**, 445–449. [in Chinese]
21. Xu L, Zhao LJ, Zhang G (2013) Turing instability in a semi-discrete Brusslator model. *Mod Phys Lett B* **27**, 1350006.
22. Mai FX, Qin LJ, Zhang G (2012) Turing instability for a semi-discrete Gierer Meinhardt system. *Physica A* **391**, 2014–2022.
23. Mistro DC, Rodrigues LAD, Petrovskii S (2012) Spatiotemporal complexity of biological invasion in a space- and time-discrete predator-prey system with the strong Allee effect. *Ecol Complex* **9**, 16–32.
24. Ghorai S, hakraborty P, Poria S, Bairagi N (2020) Dispersal-induced pattern-forming instabilities in host-parasitoid metapopulations. *Nonlinear Dynam* **100**, 749–762.
25. Ghorai S, Poria S (2016) Pattern formation and control of spatiotemporal chaos in a reaction diffusion prey-predator system supplying additional food. *Chaos Soliton Fract* **85**, 57–67.
26. Ghorai S, Poria S (2017) Impacts of additional food on diffusion induced instabilities in a predator-prey system with mutually interfering predator. *Chaos Soliton Fract* **103**, 68–78.
27. Xu L, Zhang G, Cui HY (2016) Dependence of initial value on pattern formation for a logistic coupled map lattice. *Plos One*, **11**, e0158591.
28. Zhang G, Zhang RX, Yan YB (2020) The diffusion-driven instability and complexity for a single-handed discrete Fisher equation. *Appl Math Comput* **371**, 124946.
29. Huang WH (2000) Stabilizing nonlinear dynamical systems by an adaptive adjustment mechanism. *Phys Rev E* **61**, 1011–1015.
30. Huang WH (2000) Stabilizing unstable discrete systems by a nonuniformly adaptive adjustment mechanism. *Phys Rev E* **62**, 3455–3460.
31. Zheng YA (2006) Controlling chaos using Takagi-Sugeno fuzzy model and adaptive adjustment. *Chinese Phys* **15**, 2549–2552.
32. Zheng YA (2006) Controlling chaos based on an adaptive adjustment mechanism. *Chaos Soliton Fract* **30**, 1069–1073.
33. Li T, Ma JH (2015) Complexity analysis of dual-channel game model with different managers' business objectives. *Commun Nonlinear Sci Numer Simul* **20**, 199–208.
34. Xu L, Liu JY, Zhang G (2018) Pattern formation and parameter inversion for a discrete Lotka-Volterra cooperative system. *Chaos Soliton Fract* **110**, 226–231.